Progress In Electromagnetics Research M, Vol. 114, 91–101, 2022

Tunable Dual-Band and Polarization-Insensitive Electromagnetic Induced Transparency-Like Window Based on Graphene Metamaterials

Qixiang Zhao[1], Yanyan Liang[2], Mengshi Ma[2], Hang Mo[2], Lin Peng[2], You Lv[1], and Shuquan Zheng[2, *]

Abstract—In this paper, a polarization-insensitive and dual-band Electromagnetic Induced Transparency-Like (EIT-Like) metamaterial is proposed, which is made of a cross-shaped graphene structure. Due to the mutual coupling between intralayer and interlayer, two high transmission windows can be obtained in different frequency bands. The sensibilities located at the two transmission peaks are calculated as 0.385 THz/RIU and 0.979 THz/RIU, respectively. In addition, the maximum group index of 174.5 is obtained. By adjusting the Fermi level of graphene, the transmission and group index could be modulated independently. The characteristics make the proposed metamaterials possess the potential as a tool for biological detection, slow light technology, and filters in THz region.

1. INTRODUCTION

Metamaterials are artificially designed micro-nano structures, which can achieve special characteristics such as negative refractive index and super-resolution imaging, strong absorption, etc. [1, 2]. Recently, metamaterials have been developed using artificial intelligence [3]. It is worth mentioning that metamaterials have been proposed for several emerging applications such as beam steering [4], terahertz filters/antenna-sensors [5], and near-field conversion of electromagnetic sources [6]. In recent years, it is proved that electromagnetic induced transparency (EIT) phenomenon referring to a quantum interference can be realized in metamaterials, which could be applicable to all wavebands [7–9]. The result of EIT phenomenon is a very narrow transparent window generated in the absorption spectrum. Different from EIT phenomenon in the classical three-level system, the EIT phenomenon in metamaterials could be observed because of the coupling effect between resonance units. The significance of EIT phenomenon in the metamaterial system would cause the strong dispersion induced over a narrow spectral range, which makes it very promising for biosensors and slow light devices [10–13]. For example, Rodrigo et al. reported a graphene-based tunable mid-infrared biosensor and demonstrated its potential for quantitative protein detection and chemical specific molecular identification [14]. There are two ways to achieve EIT effect. One is through the bright-bright modes coupling, and the other is bright-dark modes coupling [15]. Traditionally, EIT effect is achieved through the mutual coupling between the bright and dark modes, using metal lines and metal split rings as bright and dark modes, respectively. The bright mode can be directly excited by the incident wave to produce dipole oscillation, whereas the dark mode is difficult to be excited by the incident wave immediately, only be excited by the coupling of the bright mode. The excited dark mode suppresses the resonance of the bright mode and then produces a high transmission window [16–18]. This coupling between bright and dark modes includes

Received 24 August 2022, Accepted 27 October 2022, Scheduled 17 November 2022

* Corresponding author: Shuquan Zheng (442905738@qq.com).

[1] Guangxi Key Laboratory of Information Materials, Guilin University of Electronic Technology, Guilin 541004, China. [2] Guilin University of Electronic Technology, Guilin, Guangxi 541004, China.

intralayer and interlayer couplings. The interlayer coupling can be achieved by observing the phase change of the current or electric field between the transparent resonance point and transparent peak. In the second situation, both bright modes can be excited by the incident wave simultaneously, and the EIT is produced by mutual suppression between the two bright modes.

Graphene is a single-layer carbon atom material, which has good electrical conductivity properties, ultra-high electron mobility, and excellent stability in the terahertz range [19, 20]. Due to its reconfigurability and higher absorbance, graphene has been introduced and used to design reconfigurable antennas, absorbers, sensors, and modulators in the terahertz band [21]. Because the carrier concentration and conductivity of graphene can be dynamically controlled by chemical doping or bias voltage, graphene is widely used as modulator. Shi et al. designed a graphene nanostructure to obtain plasmonic modes with the desired radiative properties such as bright and dark modes [22]. The results show that EIT effect could be achieved by these two plasmonic modes together, and there exists very large group delay on an order of magnitude larger than that provided by the metal structure at the transparent window. Cheng et al. used graphene lines as the bright and dark modes [23], where the bright mode is placed in the middle of the two dark modes. Through moving the location of the bright mode, the EIT coupling is controlled. Xia et al. exploited surface plasmons supported by two crossed layers of graphene nanoribbons to achieve dynamically tunable EIT-like window, where each graphene nanoribbon operates as both the bright and dark modes simultaneously [24]. After that, Sun et al. also used a double-layer graphene hollow model to research the coupling of the phase coupling between intralayer and interlayer couplings [20]. Our group designed a double-layer cross hollow structure that acted as two bright modes [25]. The EIT effect is achieved because of the mutual coupling between the upper and lower layers of graphene. Through tuning the Fermi energy of graphene, a transparent window with the maximum transmissivity of 98.3% and modulation depth of 17.3% can be dynamically manipulated. In addition, the influence of the deviation of the cross-shaped center on the coupling is also studied [26]. When the electric field is incident along the X direction, a dual-band EIT effect can be achieved.

In this paper, a polarization-insensitive and dual-band EIT graphene metamaterial is proposed. The unit cell consists of double layer cross-shaped graphene, which enables the generation of two polarization-independent transparency windows. By adjusting the Fermi level of graphene, the amplitude and frequency of the dual-band transparent window can be modulated. Combined with the current density characteristic of graphene, the surface electric field and current distributions are used to explain the principle of resonance. To explore the coupling mechanism among the three bright modes, coupled Lorentz model is employed. It is shown that the coupling strength among the three bright modes will be modulated with the Fermi level changed. In order to discuss the sensitivity and slow wave effect of the proposed structure, the sensibility and group index are calculated, respectively. The proposed device shows a great potential in the field of research on polarization-insensitive, adjustable, and dual-band EIT applications.

2. STRUCTURE DESIGN

As shown in Fig. 1, the designed graphene EIT metamaterial consists of four parts, a upper layer graphene, a layer polyimide medium, a lower layer graphene, and a layer Silica medium. The upper graphene structure is made of two cross-shaped graphene strips, U1, U2, with different lengths, which are rotated by 45°. The lower graphene cross-shaped structure contains two equal-length graphene strips, L1, L2, to introduce a strong electrical resonance. The lengths of U1, U2, L1, and L2 are l_1, l_2, l_3, and l_4, respectively. The thicknesses of the polyimide and silica layers are d_1 and d_2. Both the length and width of the dielectric layer in one unit cell are l_5. The structural parameters are all listed in Table 1. The frequency domain solver of the electromagnetic simulation software CST is used to simulate the cell structure. The electromagnetic wave is incident vertically along the negative direction of z-axis, and the boundary conditions in x and y directions are chosen as unit cell.

The preparation steps of graphene metamaterials are as follows: first, a single-layer large area graphene sample is grown on copper by chemical vapor deposition (CVD) [27, 28], and then the graphene sample is transferred to the upper and lower layers of the dielectric layer by the wet chemical transfer process. Then, graphene is etched into a cross shape by ion beam lithography. Finally, two large metal

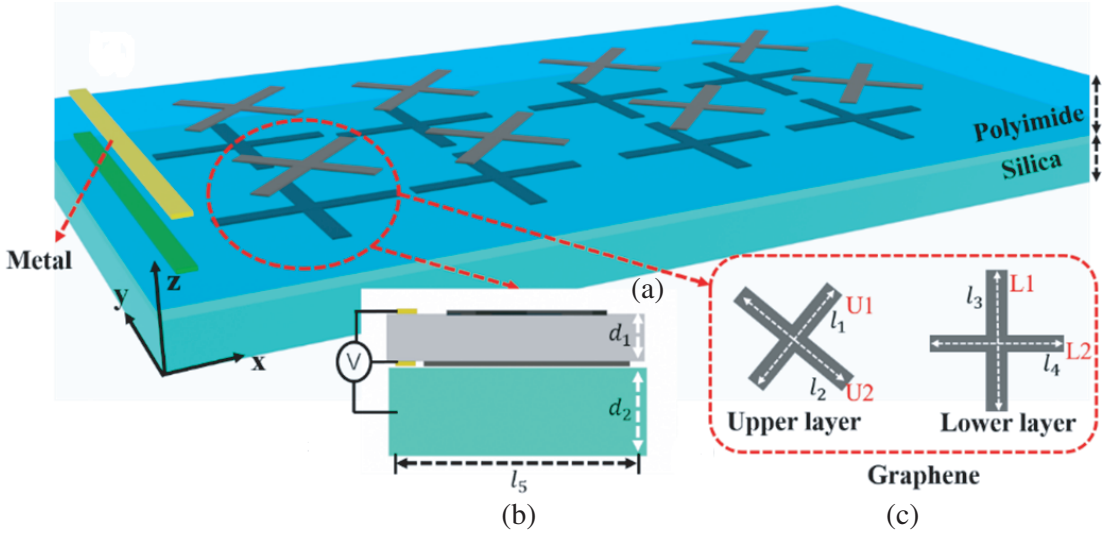

Figure 1. The geometry of the proposed double-layer cross structure structure. (a) Schematic view of array. (b) The Cross-sectional view of unit cell. (c) The Schematic diagram of the upper graphene layer and lower graphene layer.

Table 1. Geometric parameters of the unit cell.

Parameters	Value (μm)
l_1	0.8
l_2	1
l_3	1
l_4	1
l_5	1.2
d_1	0.2
d_2	0.5

electrodes are added on both sides of graphene and deposited on both ends of the sample to connect the graphene grid.

The conductivity of graphene can be expressed by Kubo formula σ=σ_{intra}+σ_{inter}, where σ_{intra} and σ_{inter} represent the intraband and interband conductivities of graphene. Because the interband conductivity in the terahertz range can be ignored, only the intraband conductivity is considered, and the conductivity of graphene can be expressed by the Drude model [29, 30]:

$$\sigma_{intra}=j\frac{e^2E_F}{\pi\hbar^2(w+j2\Gamma)} \tag{1}$$

where E_F is the Fermi energy level, and τ is the electron-phonon relaxation time. In this paper, the relaxation time of graphene is set as 2.5 ps, and E_F is in the range of 0.4–1 eV.

3. RESULTS AND DISCUSSIONS

Before discussing the proposed double-layer graphene metamaterial, the single-layer graphene structure is simulated. As shown in Fig. 2(a), it is seen that both the upper and lower graphene layers can be excited by Y-polarized incident waves, and the upper graphene layer (red line) has two resonant frequency points at 4.563 THz and 5.557 THz, while the bottom graphene layer (black line) has a

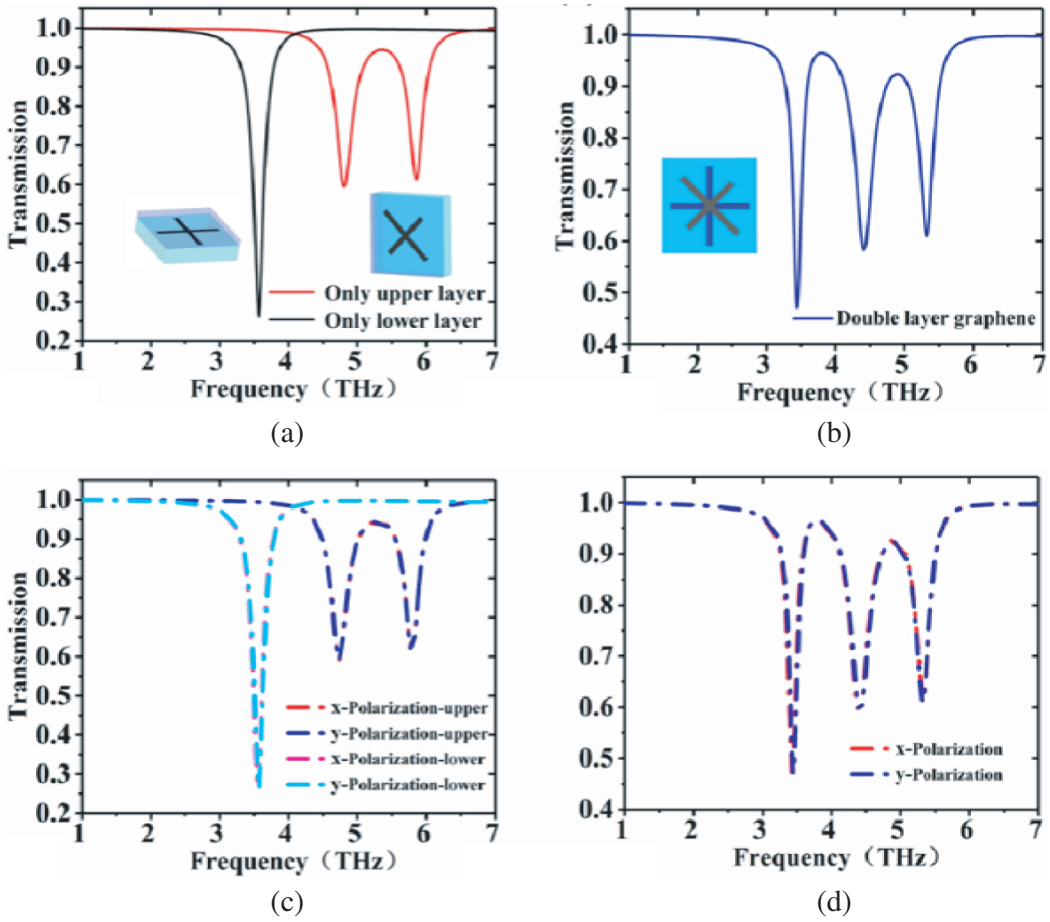

Figure 2. Simulated transmission spectra of (a) single graphene layer structure and (b) combined structure when the Fermi energy of the graphene E_F is 1 eV. (c) single graphene layer structure in x polarization and y polarization and (d) combined structure when the Fermi energy of the graphene E_F is 1 eV in x polarization and y polarization.

resonant frequency point at 3.508 THz. When the two graphene layers are combined together as shown in Fig. 2(b), a transparent window is generated at 3.794 THz because these two graphene layers are coupled to each other. From Figs. 2(c), (d), because the structure is in cross rotation symmetry, it shows that the transmission spectra under X- and Y-polarized incident waves are similar, indicating that the proposed graphene metamaterial is polarization insensitive. For simplification, the following studies focus on the Y polarized incident waves. The surface electric field and surface current distributions at some special frequency points are plotted in Fig. 3 to explain the induction effect between the upper and lower layers.

From Figs. 3(a), (b), (c), it is known that the resonance points are generated by the electric dipole resonance mode of the graphene strips L1, U1, and U2 (The centers of the upper and lower cross structures are aligned along the z-axis). Figs. 3(d), (e), (f) display the surface current distributions at the three resonance points and Figs. 3(g), (h) display the surface current distributions at the two transmission peaks, where the current flow direction is marked as arrow direction. It can be seen from formula (1) that with the increase of graphene Fermi level, graphene presents metal properties. Under the excitation of the incident wave, the dipole resonance is displayed, and the direction of current is the same. By comparison, due to the interference cancellation between the upper and lower graphene lines it is found that the directions of the current flow on L1 and U2 at the two transmission peaks are contrary to that at the resonance points, meaning that there exists near-field coupling between L1 and U2, U1 and U2, which creates the EIT-like effect.

Based on the analysis of the graphene conductivity from Eq. (1), it can be seen that the graphene

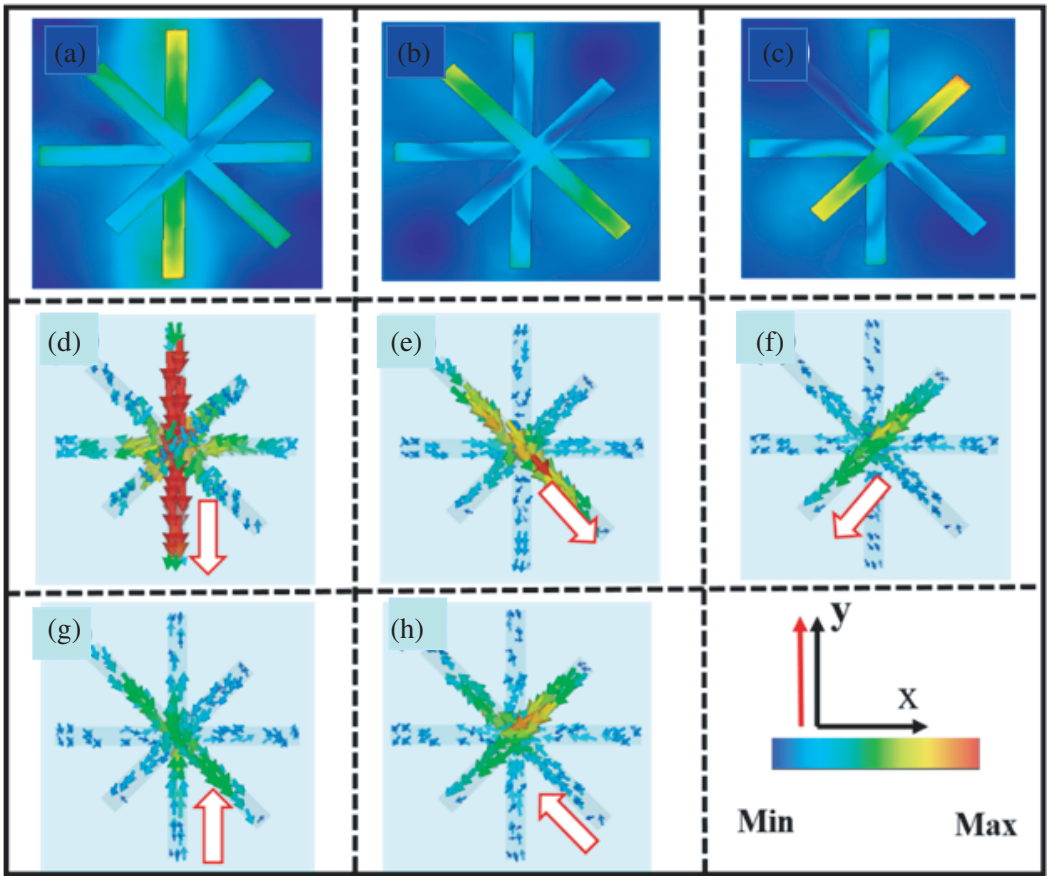

Figure 3. The (a) (b) (c) surface electric field distributions and (d) (e) (f) surface current distributions at three resonance point (3.341 THz, 4.399 THz, 5.334 TH), respectively. (g) (h) Two transparent peak points (3.794 THz, 4.905 THz) respectively.

conductivity increases with the rise of Fermi level [31]. To achieve modulation on the two transparency windows separately, the upper and lower graphene layers are applied with different bias voltages. When the Fermi level of the upper graphene is changed between $0.7 \sim 1.0$ eV, and the lower graphene is fixed at 1.0 eV, the transmission spectra are plotted in Fig. 4(a). It is shown that the second transmission peak has an obvious blue-shift in frequency. Thus, the transmission peak could be controlled by the upper graphene layer. When only the Fermi level of the lower graphene is varied between $0.7 \sim 1.0$ eV, the transmission spectra are plotted in Fig. 4(b). The first transmission peak also displays a blue-shift in frequency, meaning that the lower graphene layer can be controlled by the first transmission peak. Based on the above analysis, it is possible to independently adjust the bandwidth and peak frequency of the EIT transparent window by controlling the Fermi levels of the upper and lower graphene layers, respectively. The independent regulation of the dual-band bandwidth is achieved without changing the structure, which solves the problem of only the single-band and cannot be dynamically regulated by our team [25, 32]. It provides an effective approach for the research of dual-band independently tunable devices.

4. THEORETICAL MODEL CALCULATIONS

To explore the modulation mechanism of the dual-spectral EIT resonance, the proposed metamaterial can be quantitatively analyzed by adopting the coupled Lorentzian model. U1, U2, and L1 are directly excited by the incident electric field $E(t)$. U1 and U2 are represented by oscillators 1 and 2, and L1

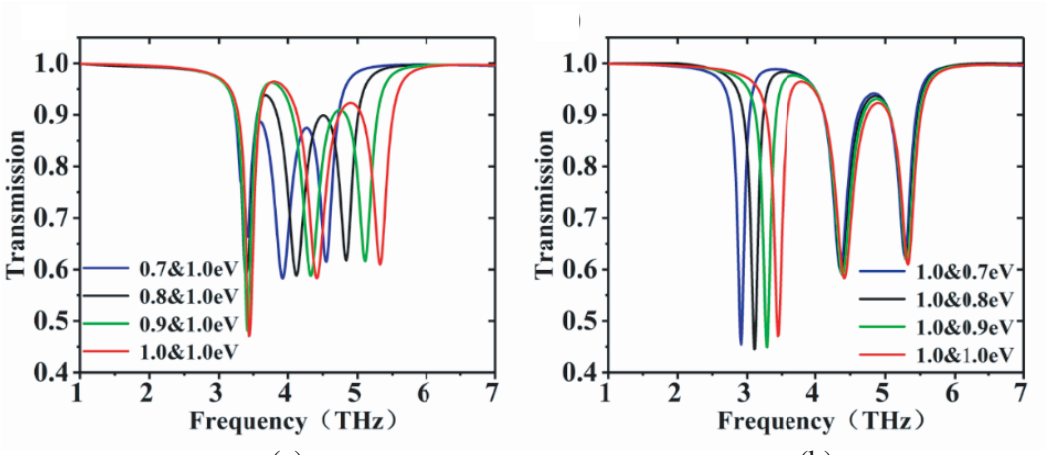

Figure 4. (a) The transmission spectra with different Fermi energies of upper graphene. (b) the transmission spectra with different Fermi energies of lower graphene layer.

is represented by oscillator 3, respectively. Similar to the three atom energy level system, when the oscillator is excited by the incident wave to generate the dipole resonance, the dipole resonance intensity will become weak due to the interference cancellation. According to the coupled differential equations, the energy dissipation of the proposed dual-spectral EIT resonance system is derived as [31, 33]

$$\begin{cases} \ddot{p}_1(t) + \gamma_2\dot{p}_1(t) + w_1^2 p_1(t) + k_1 p_2(t) = g_1 E(t) \\ \ddot{p}_2(t) + \gamma_2\dot{p}_2(t) + w_2^2 p_2(t) + k_1 p_1(t) = g_2 E(t) \end{cases} \tag{2}$$

$$\begin{cases} \ddot{p}_2(t) + \gamma_2\dot{p}_2(t) + w_2^2 p_2(t) + k_2 p_3(t) = g_2 E(t) \\ \ddot{p}_3(t) + \gamma_3\dot{p}_3(t) + w_3^2 p_3(t) + k_2 p_2(t) = g_3 E(t) \end{cases} \tag{3}$$

where γ_1, γ_2, γ_3 and w_1, w_2, w_3 are the damping factors and resonance frequencies of the U1, U2, and L1, respectively,; $E(t)=E_0 e^{iwt}$ is the incident electric field intensity with the frequency of w; k_1 is the coupling strength between U1 and U2; k_2 is the coupling strength between U2 and L1; g_1, g_2, and g_3 are the geometric parameter indicating the coupling strength of the three bright modes with incident electromagnetic field. Then above formula can be calculated [34, 35]

$$\begin{cases} (w - w_1 + i\gamma_1)p_1 + k_1 p_2 = g_1 E \\ (w - w_2 + i\gamma_2)p_2 + k_1 p_1 = g_2 E \end{cases} \tag{4}$$

$$\begin{cases} (w - w_2 + i\gamma_2)p_2 + k_2 p_3 = g_2 E \\ (w - w_3 + i\gamma_3)p_3 + k_2 p_2 = g_3 E \end{cases} \tag{5}$$

Then

$$p_2 = \frac{g_2 E(w - w_1 + i\gamma_1) - g_1 E k_1}{(w - w_1 + i\gamma_1)(w - w_2 + i\gamma_2) - k_1^2} \tag{6}$$

$$p_3 = \frac{g_3 E(w - w_2 + i\gamma_2) - g_2 E k_2}{(w - w_2 + i\gamma_2)(w - w_3 + i\gamma_3) - k_2^2} \tag{7}$$

where

$$T = 1 - \left|\frac{p_2}{E}\right|^2 - \left|\frac{p_3}{E}\right|^2 \tag{8}$$

Figure 5 plots the fitted transmission spectra according to Eq. (8). The fitting curve agrees very well with the simulation one, and the SSE (Mean Square Error of Fitting) is 0.04. Through fitting the transmission curves of the designed EIT metamaterial, the response model parameters such as g_1, g_2, g_3, k_1, and k_2 are obtained as shown in Fig. 6, and the influences of these parameters on the properties of the EIT effect are further studied. g_1, g_2, and g_3 are the geometric parameters indicating the coupling

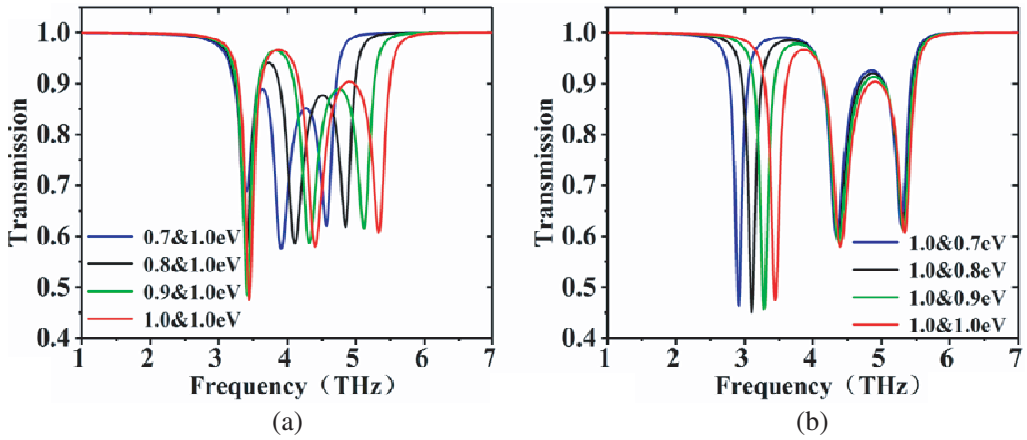

Figure 5. (a) The Fitted curve with different Fermi energies of upper graphene, and the Fermi level of lower graphene layer are 1 eV. (b) The Fitted curve with different Fermi energies of lower graphene layer, and the Fermi level of upper graphene layer are 1 eV.

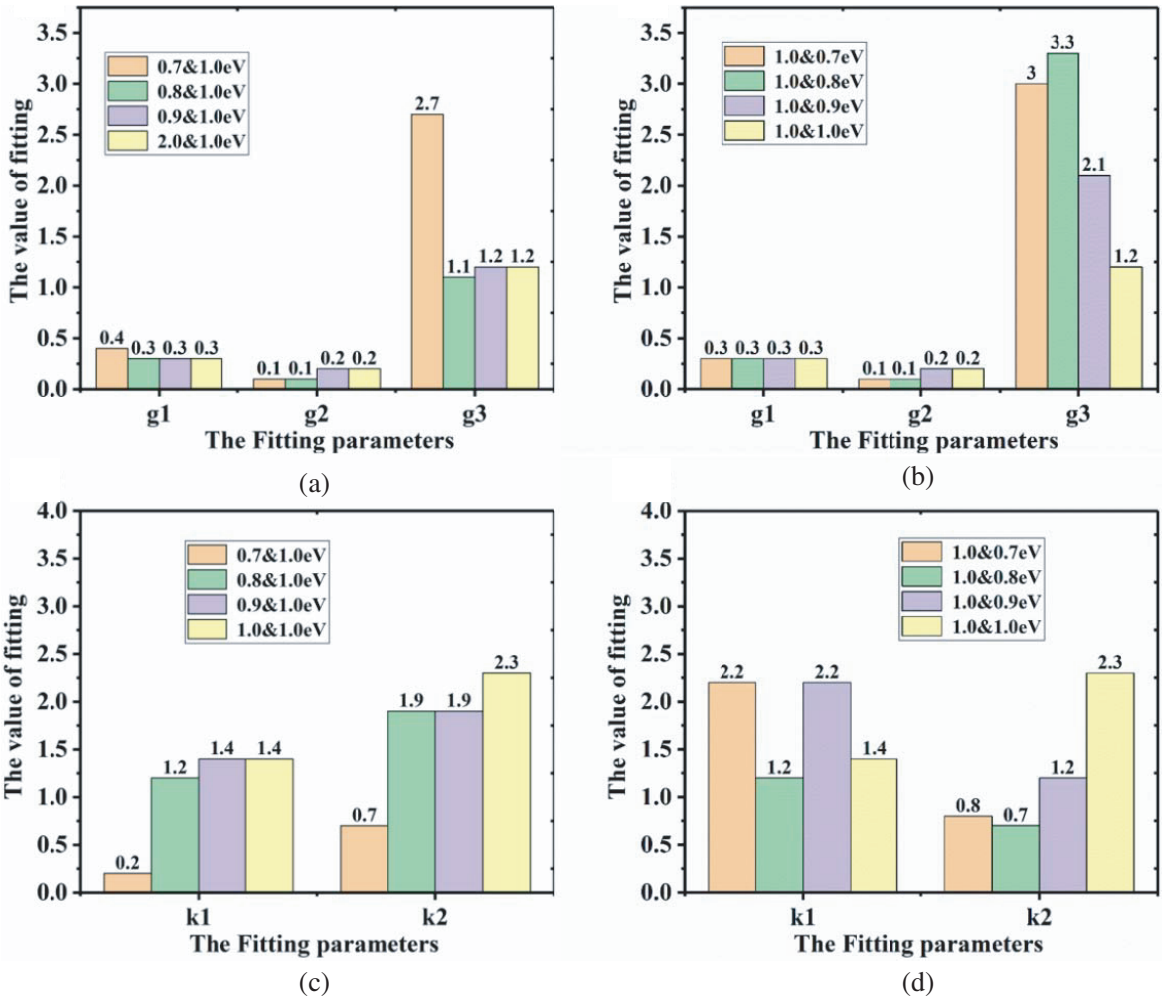

Figure 6. (a) (c) The Fitted parameter with different Fermi energies of upper graphene, and the Fermi level of lower graphene layer are 1 eV. (b) (d) The Fitted curve with different Fermi energies of lower graphene layer, and the Fermi level of upper graphene layer are 1 eV.

strength between the bright mode and incident electromagnetic field. As shown in Figs. 6(a) and (b), it can be seen that g_3 is much larger than the values of g_1 and g_2, which means that the lower graphene layer L1 is easier to be excited by incident waves to generate dipole resonance. This is the reason that when the direction of the electric field of the incident wave is along the direction of U1, a strong dipole resonance is excited as shown in Fig. 3(d). When the Fermi level of the upper graphene rises, the coupling strength among the three bright modes increases because the local surface plasmon resonance of U1 and U2 increases, thus the coupling strengths k_1 and k_2 in Fig. 6(c) gradually increase. In addition, the local surface plasmon resonance of the lower graphene becomes stronger with the increase of Fermi energy level of the lower graphene, thus the coupling strength between U2 and L1 increases, and the value of coupling strength k_1 keeps large and stable, whereas k_2 shows an increasing trend in Fig. 6(d). Through the calculation of the Lorentz model, we can get a better theoretical analysis of the simulation results.

5. REFRACTIVE INDEX SENSITIVITY ANALYSIS

The EIT structure is quite sensitive to the change of the dielectric constant of the surrounding medium, thus it can be applied to refractive index sensor [11]. In order to explore the sensitivity of the designed metamaterial, an analyte layer with a thickness of 1 μm is added on the top surface and covers the whole sensor unit. When the refractive index of the analyte is increased from 1.0 to 2.0, the equivalent dielectric constant of the surrounding medium increases correspondingly, which leads to the transparency peaks experiencing a red shift in frequency, and the amplitude has a slight decrease as shown in Fig. 7(a). The frequency of the transmission peak with different refractive indices is displayed in Fig. 7(b). It can be seen that the peak frequency linearly varies with the refractive index. The quality factor $S = \Delta f/\Delta n$ can quantify the sensitivity of the proposed EIT metamaterial. The corresponding sensitivity in peak 1 (low frequency) and peak 2 (high frequency) can reach 0.385 THz/RIU and 0.979 THz/RIU. By comparison, the sensitivity of peak 1 is lower than that of peak 2. Because the resonance field of peak 1 is mainly determined by the lower graphene layer, the change of the refractive index of the analyte has less influence on the lower graphene, which results in a smaller sensitivity coefficient of peak 1. The above analysis shows that the proposed structure has good potential for label-free bioassays.

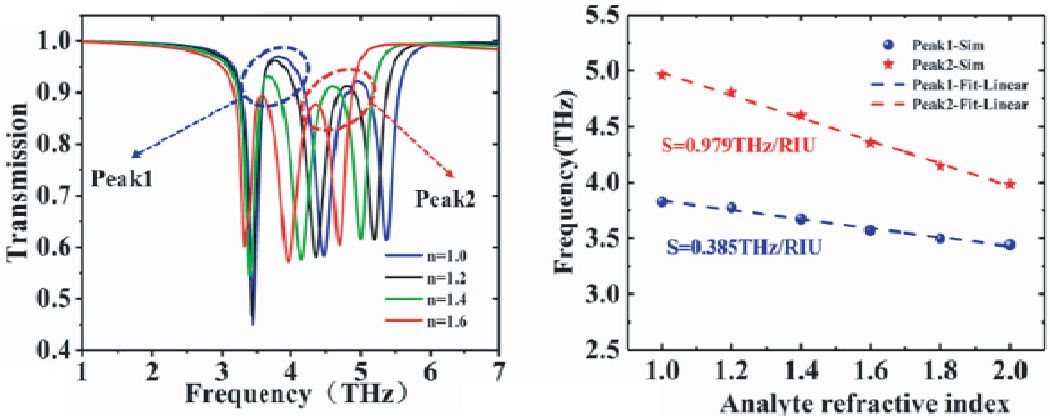

(a) (b)

Figure 7. (a) Transmission spectra of the EIT metamaterials with different refractive index of the surrounding environment. (b) Simulated dependence of the EIT metamaterials peak frequency on the refractive index.

6. GROUP DELAY CHARACTERISTICS

EIT effect can reduce the group velocity of incident light due to the strong dispersion of transmission phase around the electromagnetically induced transparent window [35, 36]. The group index can be

expressed by following equation [37]:

$$n_g = -\frac{c_0}{h} \cdot \frac{\mathrm{d}\varphi(\omega)}{\mathrm{d}\omega} \tag{9}$$

where h is the thickness of the unit structure, and $\varphi(\omega)$ is the phaseshift of the transmission. In Fig. 8(a), the Fermi energy of the upper graphene layer is 1 eV, and it can be seen that the phase shift changes with the Fermi level of the upper graphene. As shown in Fig. 8(b), the value of group index gradually rises when the Fermi energy of the lower graphene layer increases from 0.8 to 1 eV. Furthermore, the maximum group index is 175.6 at 1 eV. From the above analysis, it can be seen that the slow light effect of the PIT structure can be dynamically regulated by adjusting the graphene Fermi level.

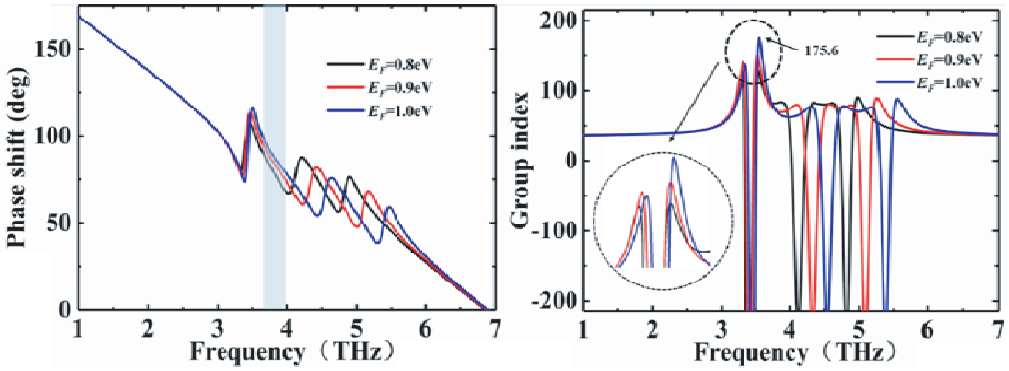

Figure 8. (a) The phaseshift of the transmission. (b) The group index of PIT metamaterial.

7. CONCLUSION

The metamaterial made of double layers to realize the EIT-Like window in the terahertz regime. Due to the mutual coupling between interlayer and interlayer, two transmission windows are generated in the transmission spectrum. Through controlling the Fermi level of graphene, the amplitude and frequency of the transparent window can be modulated. To further explain the coupling mechanism between modes, we use the coupled Lorentz model to explain the coupling mechanism among the three bright modes and the incident wave. The calculated transmission spectra have great agreement with the simulated transmission spectra. In addition, we investigated the refractive index sensing performance and slow light effect of the structure. The sensibility of the two transmission peaks was calculated as 0.385 THz/RIU and 0.979 THz/RIU, respectively, and the group index of 174.5 is obtained. Therefore, the proposed structure has good potential in detecting the surrounding environment and slowing the speed of light. This study provides a feasible solution to realize EIT analogue with the multilayer graphene coupling, and it also offers potential applications such as biological detection, slow light technology, switchers, and filters in THz regions.

Funding

The National Natural Science Foundation of China (Grant No. 62001131), Guangxi Key Laboratory of Wireless Broadband Communication and Signal Processing (Grant No. GXKL06190102), Guangxi Key Laboratory of Information Materials (Grant No. 211020-Z), and Innovation Project of GUET Graduate Education (No. 2021YCXS023).

Disclosures

The authors declare no conflicts of interest.

Data Availability Statements

The data that support the findings of this study are available from the corresponding author upon reasonable request.

REFERENCES

1. Yao, G., "Research on dynamic modulation characteristics of terahertz metamaterials based on graphene plasma induced transparency," Shanghai Jiaotong University, Shanghai, 2017 (in Chinese).
2. Dai, L. L., Y. P. Zhang, H. Y. Zhang, and J. F. O'Hara, "Broadband tunable terahertz cross-polarization converter based on Dirac semimetals," *Appl. Phys. Exp.*, Vol. 12, No. 7, 075003, 2019.
3. Lalbakhsh, A., R. B. Simorangkir, N. Bayat-Makou, A. A. Kishk, and K. P. Esselle, "Advancements and artificial intelligence approaches in antennas for environmental sensing," *Artificial Intelligence and Data Science in Environmental Sensing*, 19–38, 2022.
4. Das, P., K. Mandal, and A. Lalbakhsh, "Beam-steering of microstrip antenna using single-layer FSS based phase-shifting surface," *International Journal of RF and Microwave Computer-Aided Engineering*, Vol. 32, No. 3, e23033, 2022.
5. Esfandiyari, M., A. Lalbakhsh, S. Jarchi, M. Ghaffari-Miab, H. Noori Mahtaj, and R. B. V. B. Simorangkir, "Tunable terahertz filter/antenna-sensor using graphene-based metamaterials," *Materials & Design*, Vol. 220, 110855, 2022.
6. Lalbakhsh, A., M. U. Afzal, T. Hayat, K. P. Esselle, and K. Mandal, "All-metal wideband metasurface for near-field transformation of medium-to-high gain electromagnetic sources," *Scientific Reports*, Vol. 11, No. 1, 1–9, 2021.
7. Liu, N., T. Weiss, M. Mesch, L. Langguth, U. Eigenthaler, M. Hirscher, C. Sonnichsen, and H. Giessen, "Planar metamaterial analogue of electromagnetically induced transparency for plasmonic sensing," *Nano Letters*, Vol. 10, No. 4, 1103–1107, 2010.
8. Liu, T. T., H. X. Wang, Y. Liu, L. S. Xiao, C. B. Zhou, Y. B. Liu, C. Xu, and S. Y. Xiao, "Independently tunable dual-spectral electromagnetically induced transparency in a terahertz metal-graphene metamaterial," *J. Phys. D: Appl. Phys.*, Vol. 51, 415105, 2018.
9. Zhang, Y. D., J. Li, H. Y. Li, C. B. Yao, and P. Yuan, "Plasmon-induced-transparency in subwavelength structures," *Optics and Laser Technology*, Vol. 49, 202–208, 2013.
10. Wu, J. B., B. B. Jin, J. Wan, L. J. Liang, Y. G. Zhang, T. Jia, C. H. Cao, L. Kang, W. W. Xu, J. Chen, and P. H. Wu, "Superconducting terahertz metamaterials mimicking electromagnetically induced transparency," *Applied Physics Letters*, Vol. 99, No. 16, 161113, 2011.
11. Zhang, J., N. Mu, L. H. Liu, J. H. Xie, H. Feng, J. Q. Yao, T. A. Chen, and W. R. Zhu, "Highly sensitive detection of malignant glioma cells using metamaterial-inspired THz biosensor based on electromagnetically induced transparency," *Biosensors and Bioelectronics*, Vol. 185, 113241, 2021.
12. Yan, X., M. S. Yang, Z. Zhang, L. J. Liang, D. Q. Wei, M. Wang, M. J. Zhang, T. Wang, L. H. Liu, J. H. Xie, and J. Q. Yao, "The terahertz electromagnetically induced transparency-like metamaterials for sensitive biosensors in the detection of cancer cells," *Biosensors and Bioelectronics*, Vol. 126, 485–492, 2019.
13. Zhang, Y. G., C. Li, and X. Tu, "Tuning electromagnetically induced transparency of superconducting metamaterial analyzed with equivalent circuit approach," *Progress In Electromagnetics Research M*, Vol. 91, 29–37, 2020.
14. Rodrigo, D., O. Limaj, D. Janner, D. Etezadi, J. G. de Abajo, V. Pruneri, and H. Altug, "Mid-infrared plasmonic biosensing with graphene," *Science*, Vol. 349, No. 6244, 165–168, 2015.
15. Wang, T. L., M. Y. Cao, Y. P. Zhang, and H. Y. Zhang, "Tunable polarization-nonsensitive electromagnetically induced transparency in Dirac semimetal metamaterial at terahertz frequencies," *Opt. Mater. Express*, Vol. 9, 1562–1576, 2019.
16. Kim, T. T., H. D. Kim, R. Zhao, S. Oh, T. Ha, D. Chung, Y. H. Lee, B. Min, and S. Zhang, "Electrically tunable slow light using graphene metamaterials," *ACS Photonics: Acsphotonics*, Vol. 5, No. 5, 1800–1807, 2018.
17. Hu, Y. Z., J. You, M. Y. Tong, X. Zheng, Z. J. Xu, X. G. Cheng, and T. Jiang, "Metaphotonic devices: Pump-color selective control of ultrafast all-optical switching dynamics in metaphotonic devices," *Advanced Science*, Vol. 7, No. 14, 2070080, 2020.
18. Jin, X. R., J. Park, H. Zheng, S. Lee, Y. Lee, J. Y. Rhee, K. W. Kim, H. S. Cheong, and W. H. Jang,

"Highly-dispersive transparency at optical frequencies in planar metamaterials based on two-bright-mode coupling," *Optics Express*, Vol. 19, No. 22, 21652, 2011.

19. Peng, L., F. X. Li, X. Jiang, and S. M. Li, "A novel THz half-wave polarization converter for cross-polarization conversions of both linear and circular polarizations and polarization conversion ratio regulating by graphene," *Journal of Light Wave Technology*, Vol. 36, No. 19, 4250–4528, 2018.
20. Sun, C., J. N. Si, Z. W. Dong, and X. X. Deng, "Tunable multispectral plasmon induced transparency based on graphene metamaterials," *Optics Express*, Vol. 24, No. 11, 11466, 2016.
21. Esfandiari, M., A. Lalbakhsh, P. Shehni, S. Jarchi, M. Miab, H. Mahtaj, S. Reisenfeld, M. Alibakhshikenari, S. Kozieł, and S. Szczepański, "Recent and emerging applications of graphene-based metamaterials in electromagnetics," *Materials & Design*, Vol. 221, 110920, 2022.
22. Shi, X., D. Z. Han, Y. Y. Dai, Z. F. Yu, Y. Sun, H. Chen, X. H. Liu, and J. Zi, "Plasmonic analog of electromagnetically induced transparency in nanostructure graphene," *Optics Express*, Vol. 21, No. 23, 28438–28443, 2013.
23. Cheng, H., S. Q. Chen, P. Yu, X. Y. Duan, B. Y. Xie, and J. G. Tian, "Dynamically tunable plasmonically induced transparency in periodically patterned graphene nanostrips," *Applied Physics Letters*, Vol. 103, No. 20, 36, 2013.
24. Xia, S. X., Z. Xiang, L. L. Wang, and S. G. Wen, "Plasmonically induced transparency in double-layered graphene nanoribbons," *Photonics Research*, Vol. 6, No. 7, 31–41, 2018.
25. Zheng, S. Q., Q. X. Zhao, L. Peng, and X. Jiang, "Tunable plasmon induced transparency with high transmittance in a two-layer graphene structure," *Results in Physics*, Vol. 7, 104040, 2021.
26. Zhao, Q. X., M. S. Ma, and S. Q. Zheng, "Plasma induced transparency based on graphene super surface," *Journal of Shenzhen University Science and Engineering*, Vol. 38, No. 5, 536–542, 2021.
27. Sun, T. Y., J. Tu, Z. P. Zhou, R. Sun, X. W. Zhang, H. O. Li, Z. M. Xu, Y. Peng, X. P. Liu, P. H. Wang, and Z. C. Wang, "Resistive switching of self-assembly stacked h-BN polycrystal film," *Cell Reports Physical Science*, Vol. 3, 100939, 2022.
28. Sun, T. Y., Y. Liu, J. Tu, Z. P. Zhou, L. Cao, X. P. Liu, H. O. Li, Q. Li, T. Fu, F. B. Zhang, and Z. Q. Yu, "Wafer-scale high anti-reflective nano/micro hybrid interface structures via aluminum grain dependent self-organization," *Materials & Design*, Vol. 194, 108960, 2020.
29. Gong, Y. M., F. R. Hu, M. Z. Jiang, L. H. Zhang, Y. C. Zou, G. B. Jiang, and Y. C. Liu, "Terahertz binary coder based on graphene metasurface," *Carbon*, Vol. 184, No. 1, 2021.
30. Xu, K. D., J. X. Li, A. X. Zhang, and Q. Chen, "Tunable multi-band terahertz absorber using asingle-layer square graphene ring structure with T-shaped graphene strips," *Optics Express*, Vol. 28, No. 8, 11482–11492, 2020.
31. Sun, C., Z. W. Dong, J. G. Si, and X. X. Deng, "Independently tunable dual-band plasmonically induced transparency based onhybrid metal-graphene metamaterials at mid-infrared frequencies," *Optics Express*, Vol. 25, No. 1, 2017.
32. Zheng, S. Q., M. S. Ma, Y. Lv, T. Fu, L. Peng, and Q. X. Zhao, "Dual-band electromagnetically induced transparent metamaterial with slow light effect and energy storage," *Journal of Physics D: Applied Physics*, Vol. 55, No. 25, 255103, 2022.
33. Liu, N., L. Langguth, T. Weiss, J. Kästel, M. Fleischhauer, T. Pfau, and H. Giessen, "Plasmonic analogue of electromagnetically induced transparency at the Drude damping limit," *Nature Materials*, Vol. 8, No. 9, 758–762, 2009.
34. Artar, A., A. A. Yanik, and H. Altug, "Multispectral plasmon induced transparency in coupled meta-atoms," *Nano. Letters*, Vol. 11, No. 4, 1685–1689, 2011.
35. Jia, W., P. W. Ren, Y. C. Tian, and C. Z. Fan, "Dynamically tunable optical properties in graphene-based plasmon-induced transparency metamaterials," *Chin. Phys. B.*, Vol. 28, No. 2, 026102, 2019.
36. Kumar, D., K. M. Devi, R. Kumar, and D. R. Chowdhury, " Dynamically tunable slow light characteristics in graphene based terahertz metasurfaces," *Optics Communications*, Vol. 491, 126949, 2021.
37. Li, H. M. and Y. C. Zhang, "A low-loss, polarization-insensitive and tunable electromagnetically induced transparency," *Optical and Quantum Electronics*, Vol. 53, 643, 2021.